Journal of Molecular Liquids 364 (2022) 120045

Contents lists available at ScienceDirect

Journal of Molecular Liquids

journal homepage: www.elsevier.com/locate/molliq

# Experimental, DFT and MD simulation studies of Mordant Black 11 dye adsorption onto polyaniline in aqueous solution

Hind Hajjaoui [a], Malika Khnifira [a], Amal Soufi [a], Mohamed Abdennouri [a], Savaş Kaya [b], Recep Akkaya [c], Noureddine Barka [a,*]

[a] Sultan Moulay Slimane University of Beni Mellal, Multidisciplinary Research and Innovation Laboratory, FP Khouribga, BP. 145, 2500 Khouribga, Morocco
[b] Sivas Cumhuriyet University, Health Services Vocational School, Department of Pharmacy, 58140 Sivas, Turkey
[c] Sivas Cumhuriyet University, Faculty of Medicine, Department of Basic Medical Sciences, 58140 Sivas, Turkey

ARTICLE INFO

*Article history:*
Received 17 March 2022
Revised 3 August 2022
Accepted 4 August 2022
Available online 8 August 2022

*Keywords:*
Polyaniline
Emulsion polymerization
Dyes sequestration
DFT
Molecular dynamics

ABSTRACT

In this study, polyaniline was synthesized using two methods; in-situ polymerization using tartaric acid as a dopant (PANI/TA) and emulsion polymerization in the presence of hexadecyltrimethylammonium bromide as a surfactant (PANI/HTAB). Samples were characterized by SEM-EDX, FTIR, and XRD analyses. Subsequently, materials were evaluated for the adsorption of Mordant Black 11 (MB11) dye in aqueous media under different experimental conditions. Kinetic data were analyzed by pseudo-first-order, pseudo-second-order and intraparticle diffusion models. Equilibrium isotherm data were fitted to Freundlich, Langmuir, Temkin, and Dubinin-Radushkevich (D-R) models. Sample prepared by emulsion polymerization shows a higher monolayer capacity of 232 mg/g compared to 115.9 mg/g obtained for the sample prepared by in-situ polymerization. Thermodynamic study indicated an endothermic and spontaneous process. Besides, the adsorbents displayed good regeneration performance using 0.1 N NaOH solution. In addition, quantum chemical parameters were calculated by DFT and the agreement between these parameters and experimental observations was analyzed. Also, the interactions between the dye molecule and the PANI (001) surface were simulated by molecular dynamics (MD) simulation. It was found that the dye was adsorbed onto the PANI (001) surface in a nearby parallel position.



## 1. Introduction

Water purification and reuse is one of the most significant environmental challenges confronting humanity in the 21st century [1] due to the limitation of hydraulic sources, the rapid growth of the world's population, and water consumption rates. Therefore, the development of cost-effective, reliable, and environmentally friendly wastewater treatment technologies that would lead to the reuse of a considerable amount of effluent generated by different industries is highly recommended. Among different pollutants, dyes contribute to approximately 18–20 % of the total industrial water pollution, despite their high toxicity and hazards to the environment and human life [2–5].

Mordant Black 11 (MB11), also known as eriochrome black T, is an azo dye widely used in many industries, including textile, printing, and cosmetics. It is also used in laboratories as a complex metric detector to determine the total hardness of water [6]. This dye is known as irritant to eyes, skin, and lungs. In addition, it may induce nausea, vomiting, and gastrointestinal issues [7]. For these reasons, it is necessary to examine its removal from effluents before discharging them into the environment [8].

Several methods have been investigated in the treatment of dye's containing effluent, including precipitation, membrane separation, ion exchange, electrocoagulation, and photodegradation [9,10]. Despite being efficient, these methods are subject to several drawbacks, such as high investment, high operational costs, low efficiency, as well as the disposal problem of recyclability for real application in wastewater decontamination. On the contrary, the adsorption is a simple, effective, and economical technique that can effectively reduce the presence of several dyes in wastewater [11]. Many materials have been used, including biomaterials [12], waste materials [13], nanomaterials [14] and nanocomposites [15]. Despite all the efforts made in this direction, research in design and synthesis of cost-effective materials with excellent stability, efficiency, remarkable reusability and recyclability for ideal application in wastewater decontamination is still a subject of great interest.

Conducting polymers (Cp) such as polypyrrole, polyaniline and polythiophene have been used for various applications due to their

* Corresponding author.
*E-mail address:* barkanoureddine@yahoo.fr (N. Barka).

https://doi.org/10.1016/j.molliq.2022.120045
0167-7322/

distinguishable properties. Being one of the most important Cp, polyaniline (PANI) has attracted great interest due to its simple synthesis, thermal stability, high electrical conductivity and inexpensive monomer [16]. Furthermore, the presence of amine and imine groups provides active sites for scavenging organic and inorganic contaminants from aqueous media [17,18]. Generally, PANI is prepared using both chemical and electrochemical methods. The morphology of PANI prepared by the polymerization of aniline depends on the reaction conditions, such as the nature of the dopant, oxidant, temperature and the presence of surfactant. Therefore, different PANI nanostructures have been prepared and used for the removal of anionic and cationic dyes from aqueous media. For example, Ai et al. [19] studied the adsorption of methyl orange over PANI microspheres which exhibited a high removal capacity of 154.56 mg/g. Similarly, nanopolyaniline prepared in the presence of sodium dodecyl benzenesulfonate showed an adsorption capacity of 76 mg/g for the same dye [20]. In another study, polyaniline nanotubes were prepared under weak acidic media using acetic acid as a dopant and the material was used to remove methylene blue [21]. Lyu et al. [22] synthesized three-dimensional coral-like polyaniline hierarchical micro/nanostructures for removing acid red G dye with a high removal capacity of 310 mg/g. Likewise, Maruthapandi et al. [23] synthesized PANI by a facile carbon dot-initiated polymerization instead of an oxidant and tested it for the removal of methylene blue. PANI nanofibers synthesized with three different aromatic carboxylic acids as a dopant was reported by Mondal et al. [24]. They displayed an optimum indigo carmine dye adsorption capacity of 300 mg/g.

In this paper, PANI was synthesized by in-situ polymerization in the presence of tartaric acid as a dopant (PANI/TA) and by emulsion polymerization via hexadecyltrimethylammonium bromide surfactant (PANI/HTAB). The PANI structures were investigated by FTIR, XRD, and SEM-EDX techniques. The Mordant Black 11 (MB11) was chosen as an anionic dye to investigate the adsorption performance of the prepared PANI/TA and PANI/HTAB. To the best of our knowledge, the current study is the first investigation of MB11 adsorption over PANI. The quantum chemical descriptors (QCD) obtained by the DFT method were used to correlate and interpret the experimental results. Finally, molecular dynamics simulation was investigated to determine the energies and interactions between MB11 molecules and the PANI (001) surface.

## 2. Materials and methods

### 2.1. Materials

The chemicals used in this study were of analytical grade and were used as obtained. Aniline monomer ($C_6H_5NH_2$), tartaric acid, hexadecyltrimethylammonium bromide (HTAB), sodium hydroxide (NaOH), nitric acid ($HNO_3$), Ethanol (EtOH) and Mordant Black 11 were purchased from Sigma Aldrich (Germany). Sodium persulfate ($Na_2S_2O_8$) was supplied from Loba Chemie PVT.ltd (India).

### 2.2. Synthesis of PANI/HTAB and PANI/TA.

The general procedure for the preparation of PANI by emulsion polymerization (PANI/HTAB) is as follows: 5 mL of aniline were dispersed in 50 mL of distilled water. Afterward, 1.25 mmol of HTAB surfactant were added to the solution. The emulsion was sonicated for 30 min, and then the pH was adjusted to 3 by adding desired amount of tartaric acid. Polymerization was initiated by addition dropwise of sodium persulfate (with a molar ratio aniline/oxidant of 1) to the emulsion under stirring at 2 °C. The resulting solution was maintained in an ice bath at 2 °C under stirring for 10 h. The precipitate was centrifuged, washed with ethanol and deionized water several times, then dried at 60 °C for 24 h. The same protocol was used to synthesize polyaniline doped tartaric acid in the absence of surfactant (PANI/TA).

### 2.3. Characterization

XRD patterns were recorded on an EMPYREAN diffractometer. The data were recorded by scanning the samples in the 2θ ranges from 10° to 80°. SEM observation coupled EDX analysis were performed on a JEOL JSMIT200 spectroscope at an accelerating voltage of 20.00 kV. FTIR spectra were collected on a Perkin Elmer (FTIR-2000) spectrophotometer using KBr pellets.

### 2.4. Adsorption experiments.

MB 11 adsorption was performed in a batch system under different conditions of solution pH (2–12), agitation time (5–360 min), adsorbent dosage (0.1–1.2 g/L), initial dye concentration (25–500 mg/L) and temperature (10–50 °C). For adsorption kinetics experiments, the optimized mass of adsorbents was mixed with 250 mL of MB 11 solution of an initial concentration of 50 mg/L at 20 °C. After reaction time intervals, the solid was removed by centrifugation at 4000 rpm for 10 min, and the residual concentration of MB 11 was determined at 530 nm using a UV–vis spectrophotometer.

The removal percentage (% Removal) and the adsorbed amounts $Q_t$(mg/g) were calculated using the following equations:

$$\%\ \text{Removal} = \frac{C_0 - C_t}{C_0} \times 100 \tag{1}$$

$$Q_t = \frac{C_0 - C_t}{W} \tag{2}$$

where $C_o$ and $C_t$ represent, respectively, the initial and residual concentration at a time (t) and W(g/L) is the adsorbent mass per liter of dye solution.

For adsorbents regeneration experiments, the saturated PANI with MB11 was dispersed in different sodium hydroxide solutions from 0.1 to 2 M. Then, the solid was filtred and washed repeatedly with deionized water and dried at 60 °C for 24 h. Afterward, the solid was transferred into 100 mL of MB11 solution with a concentration of 50 mg/L. These adsorption–desorption cycles have been repeated for three consecutive cycles.

### 2.5. Error analysis

Several models were used to correlate the equilibrium, kinetics and mechanism of adsorption experimental results. For this reason, the accordance of fit of the chosen nonlinear models was evaluated by two error functions; sum of square error (SSE) and chi-square ($\chi^2$) analysis expressed mathematically by the given equations respectively:

$$\text{SSE} = \sum_{i=1}^{n} \left(q_{i,exp} - q_{i,mod}\right)^2 \tag{3}$$

$$\chi^2 = \sum_{i=1}^{n} \frac{\left(q_{i,exp} - q_{i,mod}\right)^2}{q_{i,exp}} \tag{4}$$

where $q_{i,exp}$ is the value of the experimental adsorbed capacity and $q_{i,mod}$ is the modeled value.

### 2.6. Conceptual DFT based calculations

The electronic structure properties were evaluated using quantum calculation. This helps to interpret and explain the mechanism of adsorption of an organic molecule on the polymeric surface. The HOMO and LUMO energies were calculated using the DFT method on the LanL2DZ basis set. All quantum chemical descriptors were calculated using the Gaussian 09 W program package.

Conceptual DFT (CDFT) is accepted as a powerful tool for analyzing global and local chemical reactivities of molecular systems. Parr's group introduced the aim of this theory to use simple and useful equations/approaches to predict chemical reactivity and stability. In this theory, popular quantum chemical parameters and their relations with total electronic energy (E) and the total number of electrons (N) at a constant external potential, υ(r), are given below [25]:

$$\mu = -\chi = \left(\frac{\partial E}{\partial N}\right)_{v(r)} \tag{5}$$

$$\eta = \left(\frac{\partial^2 E}{\partial N^2}\right)_{v(r)} = \left(\frac{\partial \mu}{\partial N}\right)_{v(r)} \tag{6}$$

$$\sigma = 1/\eta \tag{7}$$

where, μ is the chemical potential, χ is the electronegativity, η is the hardness and σ is the softness.

By applying the finite differences method to the above formulae, Parr derived the following equations from calculating the well-known quantum chemical parameters from the ground state ionization energy (I) and electron affinity (A) of chemical systems [26]:

$$\mu = -\chi = -\left(\frac{I+A}{2}\right) \tag{8}$$

$$\eta = I - A \tag{9}$$

$$\sigma = \frac{1}{I-A} \tag{10}$$

In organic chemistry, estimating molecules' electrophilic and nucleophilic behaviors is essential. In this way, reaction mechanisms are easily predicted. At the end of the 1990 s, Parr et al. [27] mathematically derived and introduced the electrophilicity index (ω) as:

$$\omega = \chi^2/2\eta = \mu^2/2\eta \tag{11}$$

It can be seen from this equation that the authors defined the electrophilicity index as the ratio of the square of the electronegativity to twice the hardness. Recently, Szentpaly and Kaya reinvestigated the physical basis, validity, and limitations of the Minimum Electrophilicity Principle. Here, they introduced the Maximum Composite Hardness Rule (MCHR) and noted that the second electrophilicity index ($\omega_2$), given by Eq.12, provides more compatible results with the Minimum Electrophilicity Principle compared to Parr's electrophilicity index in solid-state double exchange reactions. Szentpaly has already published some important papers showing the usefulness of the second electrophilicity index [28].

$$\omega_2 = (I.A)/(I-A) \tag{12}$$

In some papers regarding the analysis of chemical reactivity and stability, new and useful descriptors were introduced. In 2007, Gazquez et al. [29] derived the following equations from calculating the electrodonating power ($\omega^-$) and electroaccepting power ($\omega^+$) of chemical systems:

$$\omega^+ = (I+3A)^2/(16(I-A)) \tag{13}$$

$$\omega^- = (3I+A)^2/(16(I-A)) \tag{14}$$

Gomez and coworkers [30] proved that the back-donation energy ($\Delta E_{back\text{-}donation}$) of a chemical system is closely related to its absolute hardness and can be calculated from the following formula:

$$\Delta E_{back-donation} = -\eta/4 \tag{15}$$

The ionization energy (I) and electron affinity (A) of the chemical systems in this study were predicted with the help of Koopmans Theorem [31], giving the following relations:

$$I = -E_{HOMO} \tag{16}$$

$$A = -E_{LUMO} \tag{17}$$

### 2.7. Molecular dynamic simulation

Molecular dynamic (MD) simulation is an effective method for studying intra and intermolecular interactions, such as polymer-dye [32]. The MB11 dye has active sites that can interact with the PANI (001) surface. The Monte Carlo simulation was performed using the Adsorption Locator, CASTEP, and Forcite models included in the Materials Studio 8.0 software [33]. This simulation was run in a box (45*45*1) with periodic boundary conditions, and a vacuum layer (45) filled with 250 $H_2O$ and MB11 molecules. The MD simulation was carried out at NVT ensemble with an Andersen thermostat, 1 fs time step, 500 ps total simulation time with 298 K simulated temperature, and COMPASS used as the force field [34].

The interaction energy ($E_{Interaction}$) was calculated using equation (18).

$$E_{interaction} = E_{total} - (E_{surface} + E_{pollutant}) \tag{18}$$

herein, $E_{total}$ represents the total energy of the PANI surface with adsorbed MB11 molecule and water, $E_{surface}$ and $E_{pollutant}$ are, respectively, the total energy of the PANI-slab and isolated MB11 molecule. The binding energy between the dye and polymer substrate is defined as:

$$E_{binding} = -E_{interaction} \tag{19}$$

The radial distribution function (RDF or $g_{\alpha\beta}$ (r)) used to predict the distance between two atoms, α and β, is calculated by equation (20).

$$g_{\alpha\beta}(r) = \frac{V}{N_\alpha N_\beta}\left(\sum_{i=1}^{N_\alpha} \frac{n_i \beta(r)}{4\pi\, r^2 \Delta r}\right) \tag{20}$$

where N is the number of particles; $n_i$ β(r) is the total number of atoms β in the spherical distance r from atom α; and V is the volume of the simulation box.

## 3. Results and discussion

### 3.1. Adsorbents characterization

Fig. 1 shows SEM micrographs of PANI/TA and PANI/HTAB materials. From the images, it can be seen that PANI/TA displayed large rods with an unordered aggregated structure. In contrast, PANI/HTAB exhibited a well-defined nanorod structure with an average diameter of 200 nm. This morphology changes and directional growth of nanorods in the presence of the surfactant is due to the formation of a three-dimensional network from the self-assembly of aniline, tartaric acid and HTAB before the addition of the oxidant in the reaction media [35]. The chemical composition

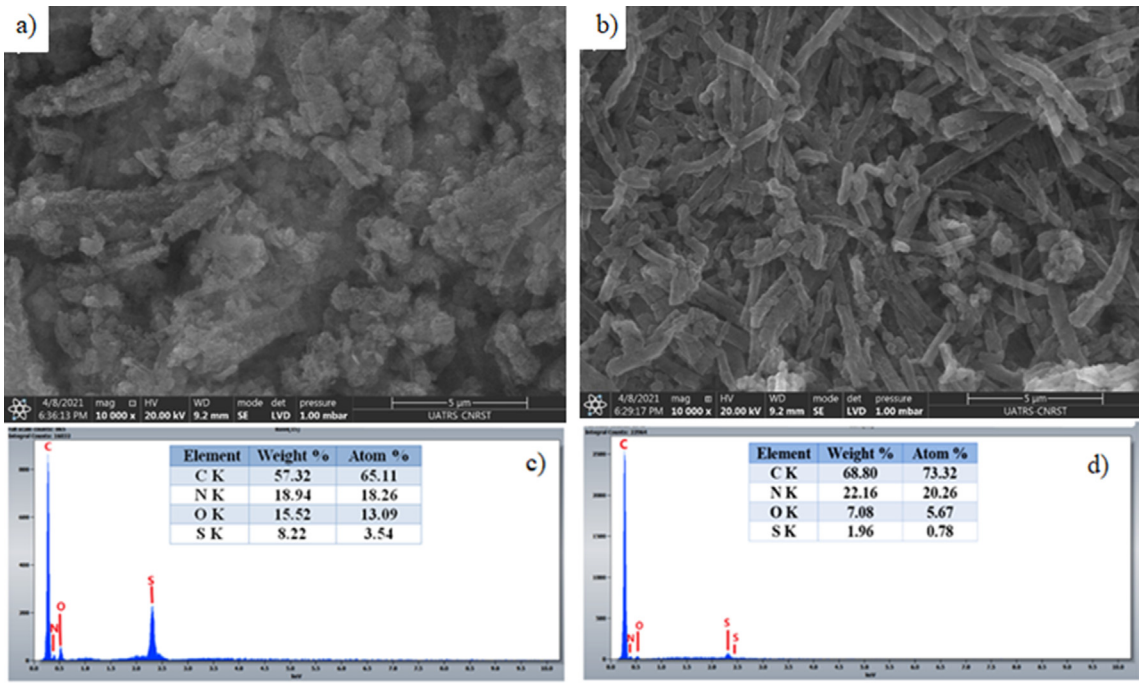


**Fig. 1.** SEM-EDX analysis PANI/TA (a,c) and PANI/HTAB (b,d).

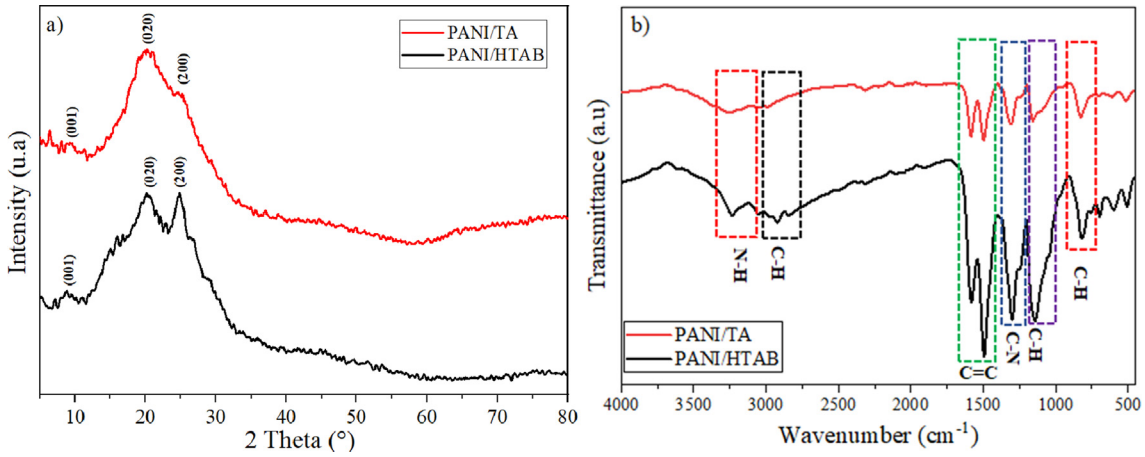


**Fig. 2.** XRD patterns (a) and FTIR spectra (b) of PANI/TA and PANI/HTAB.

of PANI/TA and PANI/HTAB was investigated using EDX analysis (Fig. 1 c-d). The results indicated that the weight percentages of C and N in PANI/HTAB are higher than in PANI/TA. This means that the polymer chain in PANI/HTAB is longer than in PANI/TA. Besides carbon and nitrogen, oxygen was also present, which is related to some moiety of tartaric acid, while sulfur may be due to the excess of sodium persulfate used as an oxidant. Fig. 2(a) illustrates the XRD patterns of PANI/HTAB and PANI/TA. As it can be seen, the XRD diffractograms of both samples look almost similar. The PANI peak diffracted at 2θ of 8.66, 20.08, and 24.94°, are indexed to the Emeraldine salt form of polyaniline [36]. The main two peaks at 2θ of 20.08 and 24.94° with a d spacing of 3.74 and 1.54 Å, indicated the low crystallinity of the prepared samples. This result is due to the repetition of benzenoid and quinoid rings in PANI chains [37].

The FTIR spectra of the materials presented in Fig. 2(b) are similar and all exhibit the distinctive bands of PANI. The band at 3241–3030 $cm^{-1}$ is assigned to the N—H stretching of an aromatic amine. The band at 2986 $cm^{-1}$ is related to an aromatic C—H stretching. The band centered at 1585–1496 $cm^{-1}$ refers to the C=C stretching deformation of benzene and quinoid rings. The 1313–1242 $cm^{-1}$ - bands correspond to C—N and C=N stretching vibrations of an aromatic amine, and peaks at 823 and 1156 $cm^{-1}$ are related to aromatic C—H out of plan bending and aromatic C—H in-plan bending. The peaks at 700 and 600 $cm^{-1}$ are assigned to the 1,3-coupling and 1,2,3-coupling of the aromatic ring, indicating that the polymer has a branched-chain structure. On the other hand, peaks in PANI/TA spectra are smaller compared to those of PANI/HTAB, suggesting that PANI/HTAB nanorods are more branched than PANI/TA. Besides, no peaks related to the stretching vibration mode of methylene or ammonium groups were present, indicating that the cationic surfactant (HTAB) has almost no chemical interaction with PANI [38]. The only observed difference between PANI/

TA and PANI/HTAB spectra is the peak intensity, indicating that PANI/HTAB has more quinonoid and benzoic rings [39]. This result is in agreement with EDX results.

### 3.2. Adsorption performance

#### 3.2.1. Effect of pH

In order to evaluate the effect of solution pH on the adsorption of MB11, experiments were done at different initial pH values in the range of 2–12. The effect of the solution pH on the removal of MB 1 by PANI/HTAB and PANI/TA adsorbents is depicted in Fig. 3. The figure indicates that the adsorption of MB11 was efficient in the pH range from 2 to 10 for both adsorbents. The decrease in MB11 adsorption in highly alkaline solutions is due to competition between $OH^-$ and MB11 ions on the adsorbent surface. In acidic media, the amine groups of PAN/HTAB and PANI/TA are protonated, which creates a strong electrostatic attraction between the positively charged emeraldine salt of polyaniline and the negatively charged ($-SO_3$) group of MB11. Moreover, polyaniline emeraldine salt is converted to emeraldine base, the neutral form of polyaniline in alkaline media [40]. From the obtained results, we can conclude that electrostatic attraction wasn't the primary mechanism responsible for MB11 adsorption onto PANI/HTAB and PANI/TA. Three mechanisms can be suggested: the bond between MB11 dye and PANI, hydrogen bonds between active sites of MB11 and amine and imine groups of the nanocomposites, and electrostatic interaction [41]. Accordingly, further experiments were performed using the initial solution pH.

#### 3.2.2. Effect of adsorbent dosage

The effect of PANI/HTAB and PANI/TA dosage on the MB11 dye uptake was studied by varying the amount of the adsorbents from 0.1 to 1.2 g/L using an initial MB11 concentration of 50 mg/L, initial solution pH, and 240 min of contact time. The results illustrated in Fig. 4 showed that increasing the adsorbent dosage from 0.1 g/L to 0.5 g/L for PANI/HTAB and from 0.1 to 0.7 g/L for PANI/TA, resulted in an increase in the removal efficiency from 43.47 to 94.27 % and from 19.82 to 68.71 %, respectively for PANI/HTAB and PANI/TA. These results could be due to an increase in the available adsorption sites [42]. However, an increase in the dosage over 0.5 g/L for PANI/HTAB and over 0.7 g/L for PANI/TA didn't change the adsorption performance. This can be explained by the decrease in mass transfer at low concentrations of dye molecules in the solution [43]. Consequently, further experiments were performed using 0.5 g/L for PANI/HTAB and 0.7 g/L for PANI/TA, respectively.

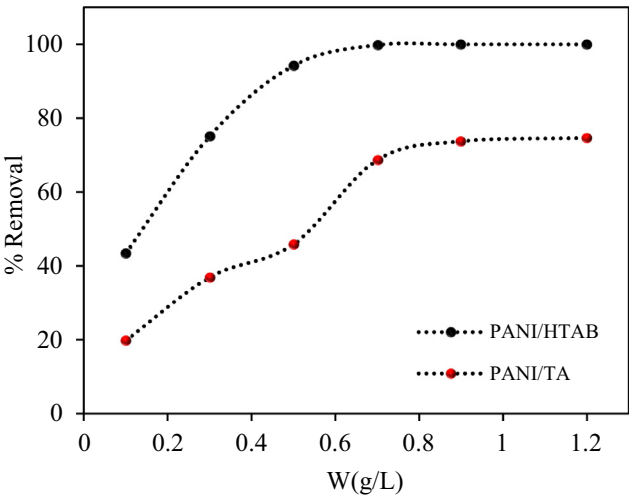


**Fig. 4.** Evolution of the MB11 removal efficiency as function of PANI samples dosage ($C_0$ = 50 mg/L, pH = $pH_i$, T = 293 K).

#### 3.2.3. Effect of the initial concentration of MB11

Fig. 5 illustrates the variation of MB11 uptake by PANI/HTAB and PANI/TA as a function of initial MB11 concentration during 240 min. The figure indicates that the removal efficiency decreased by increasing the initial concentration of MB11. This result could be explained by the saturation of the active sites of the adsorbents at high MB11 concentrations [44]. In comparison, the adsorbed amount increased from 47.68 mg/g to 233.83 mg/g and from 32.38 to 115.58 mg/g when the dye concentration was increased from 25 to 500 mg/L, respectively, for PANI/HTAB and PANI/TA. This significant improvement with increasing initial MB11 concentration could be attributed to the presence of more MB11 molecules available for the adsorbents [45].

### 3.3. Kinetic studies

The adsorption kinetic provides information about the adsorption rate, equilibrium time, and adsorbent performance. As illustrated in Fig. 6, the adsorption capacity increased by a rise in the

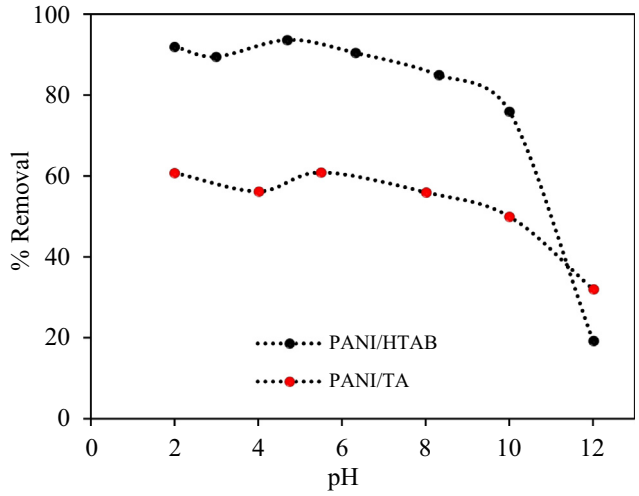


**Fig. 3.** Removal efficiency of MB11 by PANI samples as function of pH. ($C_0$ = 50 mg/L, W = 0.5 g/L, T = 293 K).

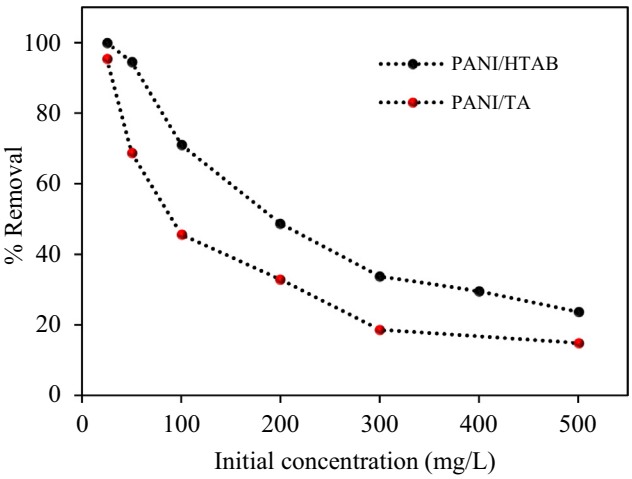


**Fig. 5.** MB11 removal by PANI/HTAB and PANI/TA as function of its initial concentration (W = 0.5 g/L, pH = $pH_i$, T = 293 K).

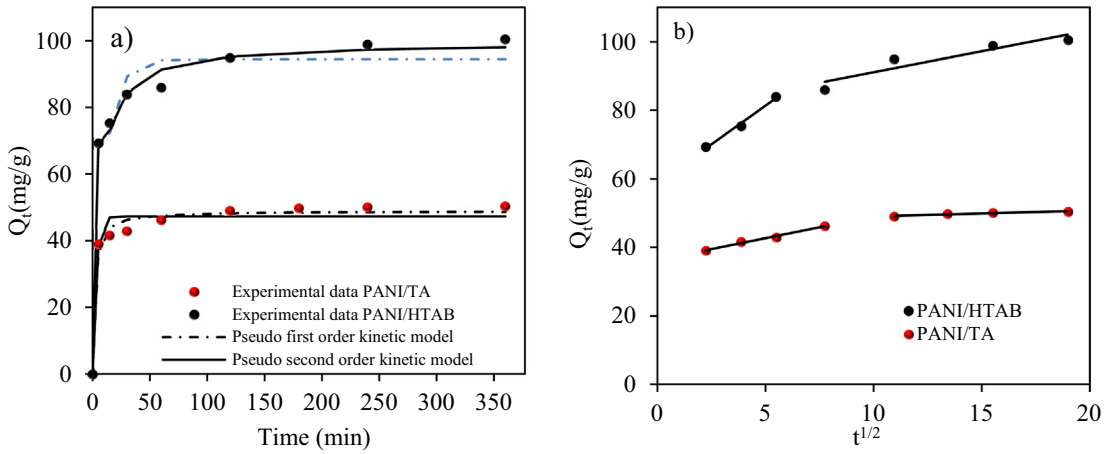


**Fig. 6.** Kinetics of MB11 adsorption by PANI/HTAB and PANI/TA (a) and Weber-Morris intraparticle diffusion plots (b).

contact time. Within the first 5 min, the uptake was fast due to the excessive number of active sites initially available on the surface of the adsorbent. However, a further decrease in the adsorption rate is observed due to a decrease in the number of active sites of PANI/HTAB and PANI/TA and the decrease of MB11 concentration in the aqueous solution [46]. The adsorption was completed within 240 min for PANI/HTAB and 180 min for PANI/TA, and the system reached equilibrium. As observed, PANI/HTAB has higher adsorption performance than PANI/TA.

To study the adsorption kinetics, the common pseudo first order and pseudo second order kinetic models were used to fit the experimental data. Pseudo first order assumes that adsorption is limited by the formation of reversible bonds between adsorbate and adsorbent active sites. Although pseudo second order takes into account chemical adsorption between adsorbate and adsorbent. The nonlinear forms of the two models can be written respectively as [47,48]:

$$Q_t = Q_e(1 - \exp^{-K_1 t}) \quad (21)$$

$$Q_t = \frac{k_2 Q_e^2 t}{1 + k_2 Q_e^2 t} \quad (22)$$

where, $k_1$(1/min) is the rate constant of the pseudo first order, $k_2$(g/mg/h) is the rate constant of the pseudo second order. $Q_e$ and $Q_t$ both in mg/g, are the amounts of MB11 adsorbed at equilibrium and at time t, respectively.

The plots of the models' curves are shown in Fig. 6(a), and their corresponding constants are recapitulated in Table 1. Based on the results, we observe that $Q_e$ calculated from pseudo second order is close to the experimental value. Moreover, the correlation coefficients $R^2$ of pseudo-second-order model are higher. On the other hand, the chi-square test and the sum of statistical analysis were applied to further investigate kinetic data. It can be observed that pseudo second order displays lower SSE and chi-square. Consequently, this model was more suitable for describing MB11 adsorption by PANI/HTAB and PANI/TA. In addition, the pseudo second rate constant for PANI/TA ($k_2$ = 1.69 $10^{-2}$) is higher than that obtained for PANI/HTAB ($k_2$ = 1.87.$10^{-3}$). Therefore, PANI/TA exhibits an excellent affinity for MB11 dye compared to PANI/HTAB. Similar findings have been reported in the literature for MB11 adsorption onto different adsorbents [49,50].

The Weber and Morris intraparticle diffusion kinetic model allows the analysis of the kinetic data and verifies whether the intraparticle diffusion is the rate-controlling mechanism of adsorption. The mathematical expression of this model can be written as [51]:

$$Q_t = \chi_i + k_i t^{1/2} \quad (23)$$

where $\chi$ is a constant related to the thickness of the boundary layer, and $k_i$ is the intraparticle diffusion rate constant (mg/g. $min^{1/2}$).

The plot of $Q_t$ versus $t_{1/2}$ illustrated in Fig. 6(b) indicated that the MB11 adsorption onto PANI/HTAB and PANI/TA involved two distinct regions. The first region represents external surface adsorption, and the second part involves intraparticle (pore) diffusion. On the other hand, the $k_1$ values are much higher than the $k_2$ values for both PANI/HTAB and PANI/TA. Therefore, external diffusion plays a significant role in the adsorption kinetics. Besides, the curve does not cross the origin (Ci-0), which explains that the intra-particle diffusion mechanism did not control the adsorption; boundary layer diffusion and external mass transfer are also involved in the adsorption of MB11 over PANI/HTAB and PANI/TA [52]. By comparing the constant rates for PANI/HTAB and PANI/TA, the adsorption on PANI/HTAB was faster.

**Table 1**
Kinetic constants for the adsorption of MB11 onto PANI/HTAB and PANI/TA.

| | Pseudo first order | | | | | | Pseudo second order | | | | |
|---|---|---|---|---|---|---|---|---|---|---|---|
| | $Q_{exp}$ (mg/g) | $Q_{e(cal)}$ (mg/g) | $k_1$ (1/min) | $R^2$ | $\chi^2$ | SSE | $Q_{e(cal)}$ (mg/g) | $k_2$ (g/mg/h) | $R^2$ | $\chi^2$ | SSE |
| PANI/HTAB | 101 | 94.46 | 0.097 | 0.978 | 1.80 | 161.61 | 99.5 | 1.87 $10^{-3}$ | 0.994 | 0.46 | 41.89 |
| PANI/TA | 50 | 47.28 | 0.338 | 0.962 | 1.70 | 76.079 | 48.95 | 1.69 $10^{-2}$ | 0.984 | 0.74 | 32.44 |
| | Intraparticle diffusion | | | | | | | | | | |
| | Initial linear portion | | Second linear portion | | | | | | | | |
| | $\chi_1$ | | $k_1$ (mg/g.$min^{1/2}$). | $R^2$ | $\chi_2$ | $k_2$ (mg/g.$min^{1/2}$). | $R^2$ | | | | |
| PANI/HTAB | 58.805 | | 4.508 | 0.989 | 136.953 | 1.2287 | 0.871 | | | | |
| PANI/TA | 36.372 | | 1.2636 | 0.989 | 47.443 | 0.1635 | 0.904 | | | | |

### 3.4. Isotherm and thermodynamic studies

In order to analyze the adsorption equilibrium data, Langmuir, Freundlich, Temkin, and Dubinin isotherm models were investigated. The Langmuir isotherm model assumes a homogeneous surface coverage of the adsorbent and is expressed as follows [53]:

$$Q_e = \frac{Q_m B_L C_{eq}}{1 + B_L C_{eq}} \quad (24)$$

where $C_{eq}$ (mg/L) is the MB11 equilibrium concentration, $Q_e$ (mg/g) and $Q_m$ (mg/g) are the adsorbed amounts at equilibrium and at saturation, respectively, and $B_L$ is the equilibrium constant that is related to the energy of adsorption.

The separation factor $R_L$ is used to judge if the adsorption system is favorable or not favorable and is given by [54]:

$$R_L = \frac{1}{1 + B_L C_0} \quad (25)$$

where $C_0$ (mg/L) is the initial MB11 dye concentration. When $R_L = 0$, the adsorption is irreversible; ($0 < R_L < 1$), the adsorption is favorable; $R_L = 1$, linear adsorption, and $R_L$ greater than 1, the adsorption is unfavorable.

The Freundlich isotherm considers that adsorption occurs on a heterogeneous surface and assumes multilayer adsorption [55]. This model is mathematically expressed by:

$$Q_e = k_f C_e^{1/n} \quad (26)$$

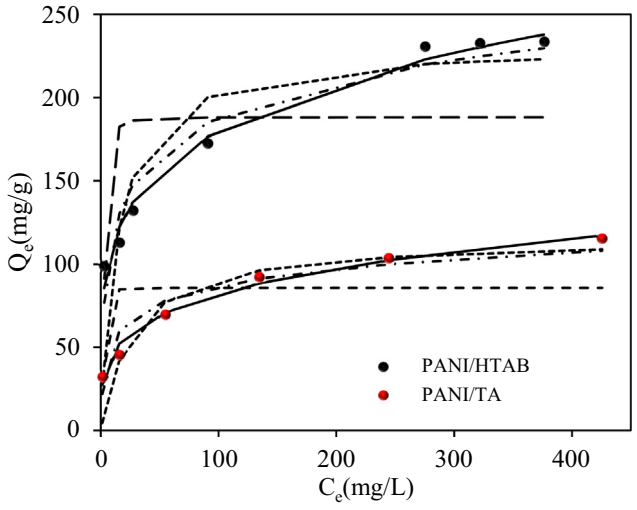


**Fig. 7.** Non-linear plots of isotherm models for MB11 adsorption onto PANI/HTAB and PANI/TA.

where, $k_f$ ($mg^{-1/n}L^{1/n}g^{-1}$) and n are the Freundlich model parameters related to adsorption capacity and intensity.

The Temkin isotherm assumes that the adsorption energy decreased linearly with the adsorbent coverage. This model is defined as:

$$Q_e = \frac{RT}{b_T} \mathrm{Ln}(AC_e) \quad (27)$$

where, R is the universal gas constant, and T is the temperature in (K). A (L/g) is related to the equilibrium binding constant, and the $b_T$ isotherm constant is linked to the heat of adsorption.

The Dubinin-Radushkevich isotherm considers a Gaussian energy distribution onto the heterogeneous surface of the adsorbent [56]. The D-R isotherm model is given by [57]:

$$Q_e = Q_m \exp(-\beta\varepsilon^2) \quad (28)$$

where $Q_m$ is Dubinin-Radushkevich adsorption capacity, β is a constant coefficient related to mean adsorption energy ($mol^2/kJ^2$), and ε is Polanyu potential expressed as follows:

$$\varepsilon = RT\mathrm{Ln}\left(1+\frac{1}{C_{eq}}\right) \quad (29)$$

To evaluate if the adsorption of MB11 is chemical or physical adsorption, the free energy of adsorption E (kJ/mol) was calculated as follows:

$$E = \frac{1}{\sqrt{2\beta}} \quad (30)$$

The plots of the nonlinear equation of the isotherm models are illustrated in Fig. 7. Besides, the parameters of each model are provided in Table 2.

The comparison of regression coefficient values and error analysis for the studied isotherms showed that MB11 adsorption on PANI/HTAB and PANI/TA follows this order: Freundlich > Temkin > Langmuir > Dubbibin-Radushkevich. Therefore, the adsorption obeys the Freundlich hypothesis and consequently PANI/HTAB and PANI/TA surfaces contain heterogeneous active sites. The maximum monolayer adsorption capacities calculated from Langmuir were 232 and 115.9 mg/g, respectively, for PANI/HTAB and PANI/TA. Besides, the n values obtained from the Freundlich isotherm are higher than 1. In the case of the Langmuir isotherm, $R_L$ is between 0 and 1, indicating favorable adsorption of MB11 on PANI/HTAB and PANI/TA. Further, the calculated values of the adsorption heat are<20 kJ/mol, suggesting a physisorption process [58]. The $B_L$ value related to PANI/HTAB is higher than that for PANI/TA, indicating higher binding energy between MB11 and PANI/HTAB than between MB11 and PANI/TA [59]. $E_{ads}$ calculated from Eq.30 were 609.75 and 1079.58 J/mol (E < 8 kJ/mol), respectively for PANI/TA and PANI/HTAB, confirming the physical adsorption of MB11 onto both PANI/TA and PANI/HTAB [60].

To study the thermodynamics of the adsorption of MB 11 on PANI/TA and PANI/HTAB, Gibbs free energy (ΔG°), enthalpy

**Table 2**
Isotherm parameters for MB11 adsorption over PANI/HTAB and PANI/TA.

| Adsorbent | Langmuir | | | | | | Freundlich | | | | |
|---|---|---|---|---|---|---|---|---|---|---|---|
| | $Q_m$ (mg/g) | $B_L$ (L/mg) | $R_L$ | $R^2$ | SSE | $\chi^2$ | n | $K_f$ ($mg^{-1/n}L^{1/n}g^{-1}$) | $R^2$ | SSE | $\chi^2$ |
| PANI/HTAB | 232 | 0.0709 | 0.03/0.22 | 0.757 | 5183.9 | 101.54 | 4.77 | 68.740 | 0.982 | 386.7 | 3.4 |
| PANI/TA | 115.9 | 0.0368 | 0.05/0.52 | 0.836 | 895.2 | 165.90 | 4.08 | 26.623 | 0.984 | 87.9 | 1.2 |
| | Temkin | | | | | | Dubinin-Radushkevich | | | | |
| | $Q_{exp}$ (mg/g) | $b_T$ (J/mol) | $A_t$ | $R^2$ | SSE | $\chi^2$ | $Q_m$ (mg/g) | E (J/mol) | $R^2$ | SSE | $\chi^2$ |
| PANI/HTAB | 233.8 | 77.88 | 4.12 | 0.936 | 1355.4 | 11.70 | 188.3 | 609.75 | 0.349 | 13,905 | 75.1 |
| PANI/TA | 115.6 | 167.62 | 3.99 | 0.917 | 3050.5 | 35.75 | 90.80 | 1079.5 | 0.442 | 454.3 | 9.8 |

**Table 3**
Thermodynamic parameters for MB11 adsorption onto PANI/HTAB and PANI/TA.

| Thermodynamic parameters T(K) | ΔG° kJ/mol 283.8 | 293.6 | 303.7 | 312.6 | 323 | ΔH° kJ/mol | ΔS° kJ/mol·K |
|---|---|---|---|---|---|---|---|
| PANI/TA | −4.66 | −7.29 | −9.99 | −12.32 | −15.17 | 71.40 | 0.27 |
| PANI/HTAB | −2.35 | −3.29 | −4.33 | −5.38 | −6.43 | 27.45 | 0.10 |

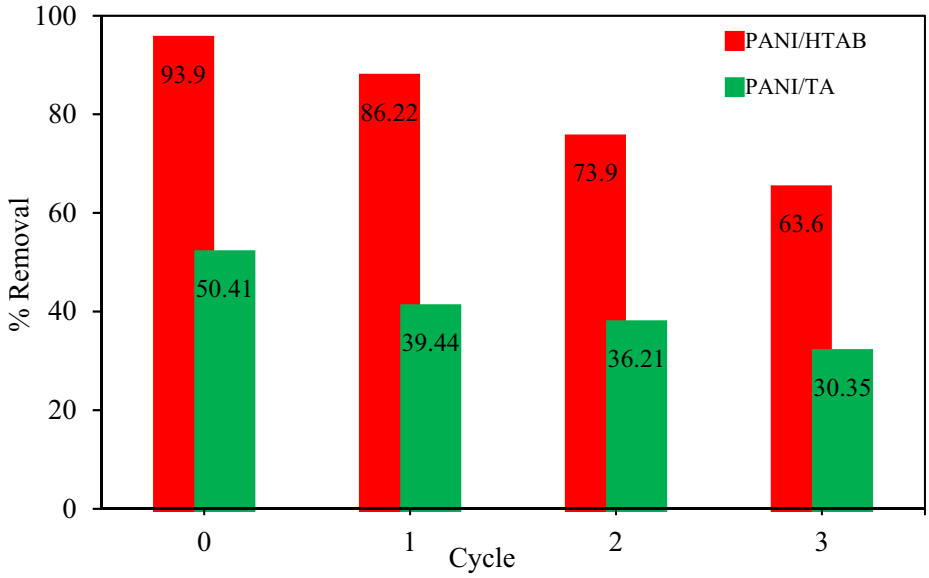


**Fig. 8.** Regeneration of PANI/HTAB and PANI/TA using NaOH 0.1 N.

(ΔH°), and the entropy (ΔS°) changes were calculated using the following equations [61]:

$$\Delta G = R\,T\,\ln(K_L) \tag{31}$$

$$\ln(K_L) = -\frac{\Delta G}{RT} = \frac{\Delta S}{R} - \frac{\Delta H}{RT} \tag{32}$$

where R is the universal gas constant, T is the temperature of the solution (K), and KL is defined as the distribution coefficient expressed as: $K_L = \frac{Q_e}{C_e}$.

Table 3 demonstrates that the ΔG values at all temperatures are negative, indicating that the MB11 molecules were spontaneously adsorbed on PANI/HATB and PANI/TA surfaces, and that the reaction is thermodynamically feasible. The positive values of ΔH suggest an endothermic adsorption process. Besides, the positive values of ΔS indicate that randomness increased at the PANI/TA or PANI/HTAB-MB11 solution interface during the adsorption.

### 3.5. Regeneration

After MB11 dye adsorption, PANI/HTAB and PANI/TA were regenerated in three NaOH solutions with concentrations of 0.1, 1 and 2 mol/L. The result indicates that the highest NaOH concentration displayed the highest desorption percentage, with no significant enhanced percentage compared to low concentration. However, considering the cost of the process, the desorption was carried out using 0.1 N NaOH solution. As shown in Fig. 8, the removal efficiency slightly decreased after each cycle, which can be explained by the irreversible blockage of some adsorbent's active sites after adsorption. Hence, PANI/TA and PANI/HTAB materials could be used repeatedly with a slight loss in MB11 dye removal efficiency.

### 3.6. Comparison with other reported adsorbents

A comparison study between the obtained result from the present study and different reported results of MB11 dye adsorption using other materials is illustrated in Table 4. The table indicates that PANI/HTAB nanorods display high removal capacity for MB11 dye adsorption compared to PANI/TA and many other adsorbents. Therefore, PANI/HTAB is an efficient adsorbent with enhanced structural properties for MB11 adsorption.

**Table 4**
Comparison of the adsorption capacities of PANI/HTAB and PANI/TA with other adsorbents.

| Adsorbent | $Q_m$ (mg/g) | Reference |
|---|---|---|
| Chitin | 167.31 | [62] |
| Ni/Al Layered double hydroxide | 37.71 | [63] |
| Alginate/basil seed mucilage biocomposite | 9.52 | [45] |
| Waste rice hulls | 160.36 | [64] |
| Ceria decorated porous diatom-xerogel | 42.07 | [65] |
| CTAB@ZnO | 59.16 | [14] |
| Polyaniline–Zirconium phosphoborate nanocomposite | 72.70 | [66] |
| $CoFe_2O_4$ | 82.6 | [67] |
| Hemoglobin/$Fe_3O_4$ | 178.6 | [68] |
| Polyaniline/ZnO nanocomposites | 18.69 | [41] |
| Magnetic graphene oxide | 210.53 | [69] |
| Graphene | 102.04 | [70] |
| PANI/HTAB | 232 | This study |
| PANI/TA | 115.9 | This study |

### 3.7. Electronic structure analysis by DFT

The electronic structure analysis based on the DFT theorem was used to investigate the adsorption behavior of MB11 onto the PANI (001) surface. The optimized structures, HOMO and LUMO orbitals, molecular electrostatic potential (MEP) and electrostatic potential (ESP) 2D maps of MB11 dye and PANI are shown in Fig. 9. The LUMO and HOMO densities of the MB11 molecule are apparently distributed over some atoms; the LUMO is located in the nitro group. In contrast, the HOMO is located on carbon atoms (*C*2, C3, C4, C5, C9, C10). Fig. 9 (b) and (c) show that both HOMO and LUMO orbitals were scantily distributed on the nitrogen atoms of the PANI, which suggests that these sites could be probable active sites of interaction.

The ESP and MEP can confirm these findings. In general, the MEP surface analysis gives a visual outline for understanding the reactive sites of molecular systems [71]. Moreover, MEP is important in designing efficient receptors for anion binding [72]. As shown in Fig. 9 (d) and (e), ESP is characterized by blue and red colors that stand for the positive and negative electrostatic potential regions, respectively. It is clear that the total density (red color) is located on the oxygen and nitrogen atoms. The O32, O33, and O37 atoms of the $-SO_3^-$ group are rich in electrons, which facilitate the sharing phenomenon with atoms poor of the electrons in

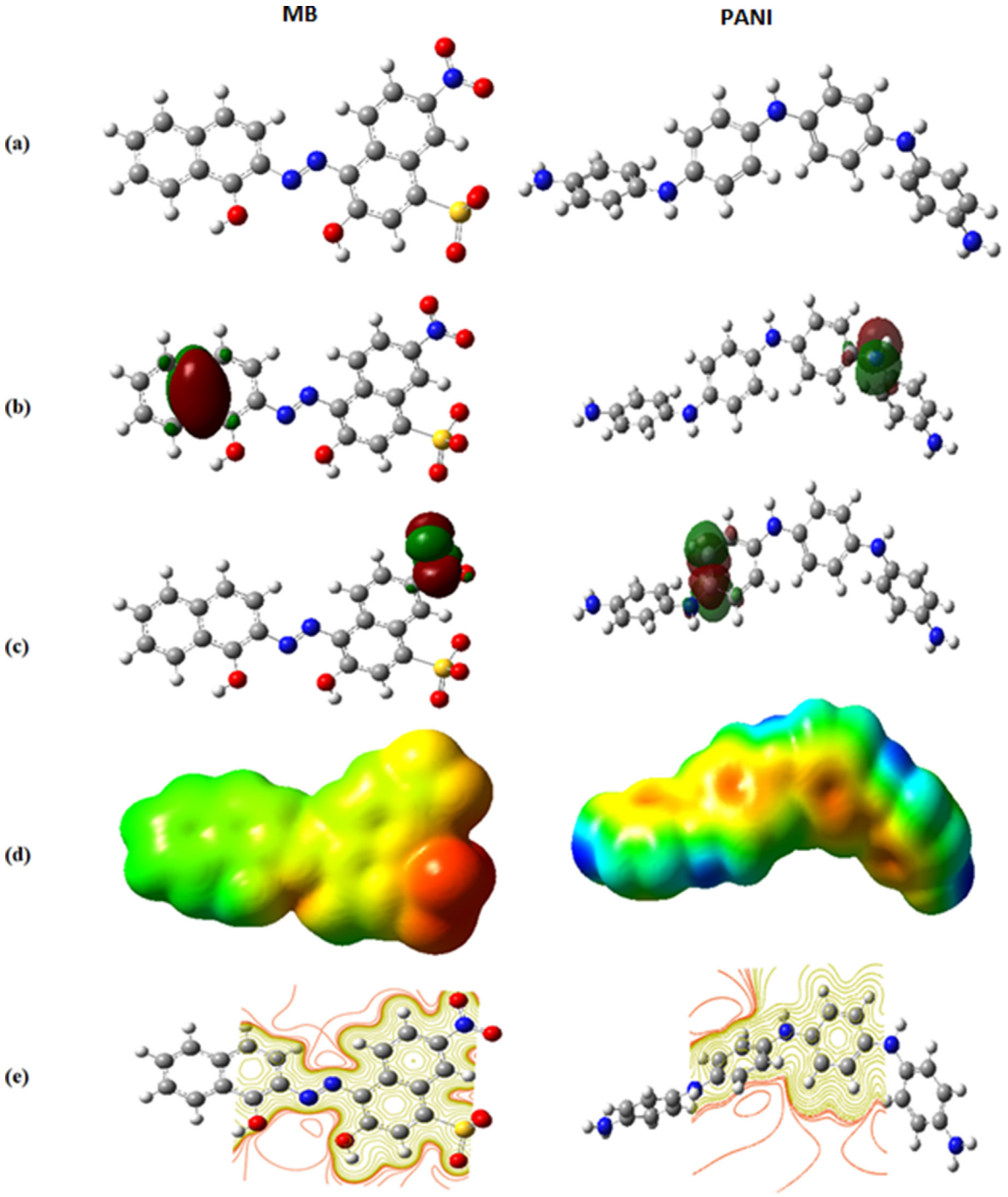


**Fig. 9.** Optimized structure (a), HOMO (b), LUMO (c), MEP (d) and ESP (e) of molecular systems.

**Table 5**
Values of the quantum chemical descriptors of MB11 and PANI.

| Quantum chemical descriptors | MB11 | PANI |
|---|---|---|
| $E_{Total}$ (eV) | −39999.7 | −32709.2 |
| DM (Debye) | 37.703 | 1.321 |
| $E_{HOMO}$ (eV) | −5.978 | −6.608 |
| $E_{LUMO}$ (eV) | −3.483 | 0.812 |
| $\chi$ | 4.73 | 2.89 |
| $\eta$ | 2.49 | 7.42 |
| $\omega$ | 4.48 | 0.56 |
| $\omega_2$ | 8.34 | −0.72 |
| $\omega^+$ | 6.75 | 0.14 |
| $\omega^-$ | 11.49 | 3.044 |
| $\Delta E_{b\text{-}d}$ | −0.62 | −1.85 |

polyaniline. The results also show that the negative regions of the MEP and ESP, red and yellow were located on the benzene rings, which are the most appropriate for electrophilic attacks. Also, it is evident from Fig. 9 (d) and (e) that the nitrogen atoms in PANI have the majority of the positive charges.

Quantum chemical parameters calculated are presented in Table 5. The HOMO and LUMO orbitals play a fundamental role in the qualitative interpretation of chemical reactivity. The values and signs of the frontier orbital coefficients are an important clue to favoring the attack mode. Thus, the electrophilic attack reagent will preferentially occur at the site with the most significant coefficient in HOMO. Alternatively, the nucleophilic attack will prefer-

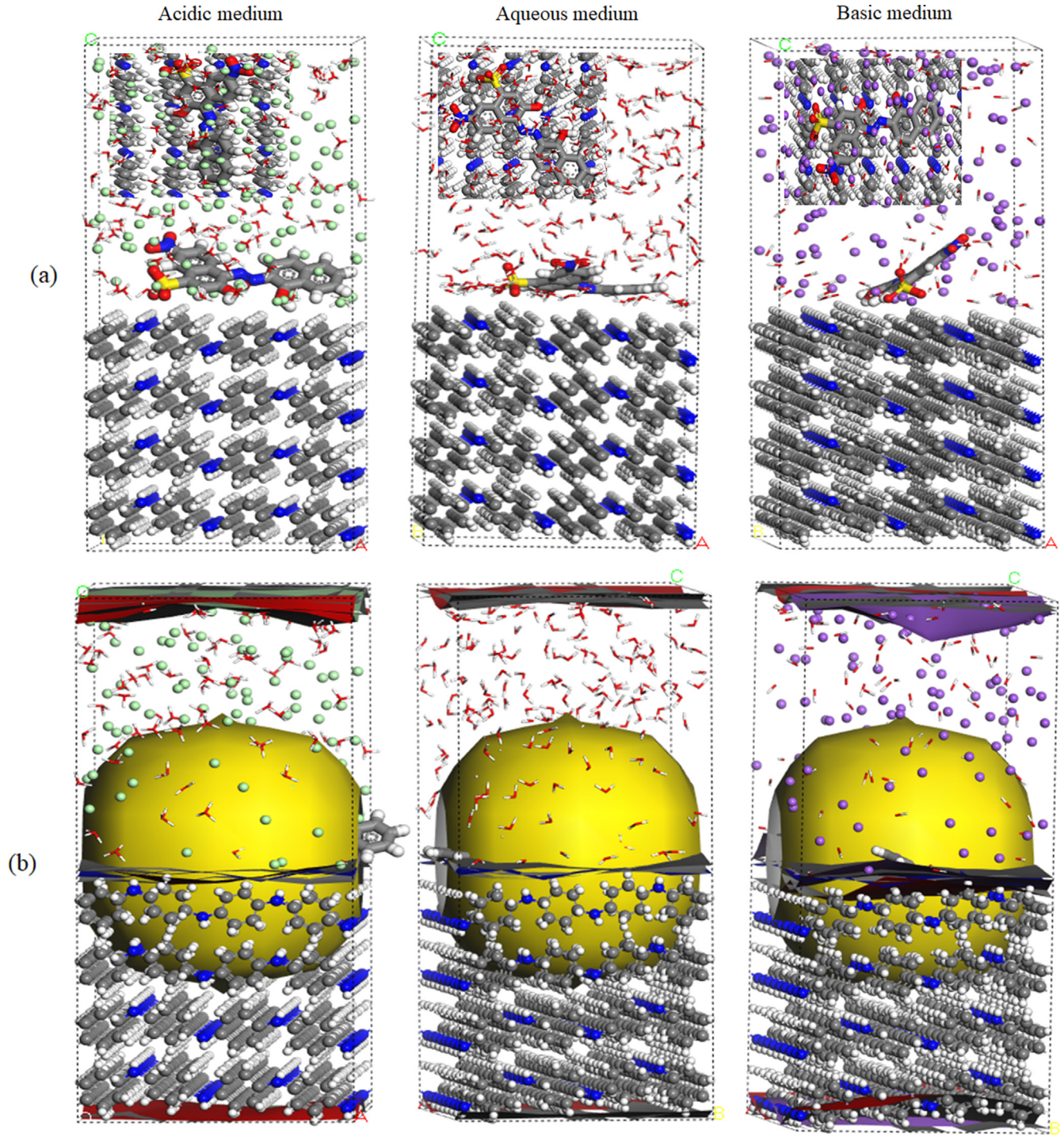


**Fig. 10.** Most stable low energy configurations for MB11 adsorption on PANI (001) surface in three mediums (Inset: on-top view) (a) and Density field distribution (b).

ably take place on the molecular sites with the highest LUMO density values. Usually, the stability and the reactivity of a molecular system can be evaluated by the total energy; a low value of $E_{Total}$ indicates low stability and more reactivity. Moreover, the calculation of the energy gap characterizes the chemical reactivity and the kinetic stability, which is also in favor of a stable MB11 adsorption onto the PANI surface. A molecule possessing a low value of $\Delta E_{gap}$ is polarizable and associated with high reactivity and low kinetic stability and is called a soft molecule. The low $\Delta E_{gap}$ is associated to MB11 molecule with a value of 2.495 eV, so MB11 is less stable and more reactive. The low value of $E_{LUMO}$ indicates stronger electronic acceptance capacity, which allows MB11 to more easily accept electrons from PANI and to form an anti-bond orbital.

The dipole moment (μ) is associated with the adsorptive capacity. The high value of μ can facilitate electrons transfer from the MB11 dye to the PANI surface. In addition, the MB11 adsorption on the PANI surface resulted in the modification of the size and direction of the μ vector. Moreover, the softness and global hardness values can determine the chemical reactivity and stability. Chemical hardness indicates the resistance of a molecular system to electron transfer. Generally, low values of the global hardness and elevated values of the global softness of a molecule can help its adsorption process on an appropriate surface. Furthermore, the electrophilicity index (ω) indicates the capability of MB11 to capture electrons. The adsorption capacity can be increased with the decrease of the ω values [73]. Then, the positive value of ΔNmax (1.896) shows the highest capacity of MB11 to give electrons to the PANI surface [74].

In the analysis of the reactivity and stability of chemical systems, the maximum hardness, minimum polarizability, and minimum electrophilicity principles are widely used. Chemical hardness is the resistance against the polarization of the electron cloud of atomic and molecular systems [75]. This concept, introduced by Pearson [76], is quite useful in estimating the nature of the interactions between chemical species. The maximum hardness principle (MHP) states that "There seems to be a rule of nature that molecules arrange themselves to be as hard as possible" [77]. It can be easily understood from this explanation that MHP presents a remarkable relationship between stability and hardness. The lower chemical hardness value supports the idea that MB11 acts as an effective electron donor against PANI. According to the minimum polarizability principle (MPP) of Chattaraj, in a stable state, polarizability is minimized [78]. Some authors noted that the dipole moment could be considered a measure of polarizability. A high dipole moment value for MB11 implies that this molecule is a reactive. Another electronic structure principle is the minimum electrophilicity principle. A few years later, after introducing the minimum polarizability principle, Chamorro, Chattaraj, and Fuentealba laid the foundation of the minimum electrophilicity principle, which suggests that in a stable state, electrophilicity is minimized like polarizability [79]. The minimum electrophilicity principle also predicts the high reactivity of MB11 like MHP and MPP. In summary, the calculated quantum chemical parameters indicated the high electron transfer from MB11 to the PANI surface, confirming the experimental findings.

### 3.8. MD simulation

MD simulation was used to understand and interpret the interactions between the MB11 and the PANI surface. Fig. 10 shows the most stable equilibrium configurations of the adsorption of MB11 molecule onto the PANI (001) surface in various mediums. The figure shows that the MB11 adsorption on the PANI (001) surface was parallel, confirming the strong interactions. The analysis of the molecular structure of MB11 and PANI indicates that MB11 adsorption onto the PANI surface can be related to the contribution of the electrons of oxygen and nitrogen. Moreover, the aromatic rings of MB11 in parallel interaction mode can support the maximum coverage. The analysis of density field of MB11 molecule on a PANI (001) substrate (Fig. 10 (b)) indicates that the dye was effectively adsorbed on the PANI surface by forming a strong bond. This condition supports the high adsorption capacity of the anionic dye by polyaniline.

Furthermore, the radial distribution function (RDF) (or pair correlation function; g(r)) is a useful method for estimating the length of the bond between the molecule and the substrate. The peaks between 0.25 Å and 3.5 Å correspond to chemisorption, while the coulomb and Van der Waals interactions are associated with peaks greater than 3.5 Å [80]. Fig. 11 shows that the distance between the oxygen (O) heteroatom of the MB11 and the nitrogen (N) atoms of the PANI (001) is near 1.15 Å, which suggests that chemical bonds can be formed between this dye and the PANI surface in the three mediums. This result confirmed the greater ability of PANI to adsorb MB, which is due to its greater ability to donate and accept electrons to the PANI surface. Moreover, the Van Der Waals dispersion forces can also contribute to catching the MB11 molecule towards the polymer surface (physical adsorption), which confirms the results obtained in the experimental results. X-ray analysis of the MB11-PANI complex in three media is shown in Fig. 12. Big X-ray scattering angle characterizes the structures of the compounds obtained.

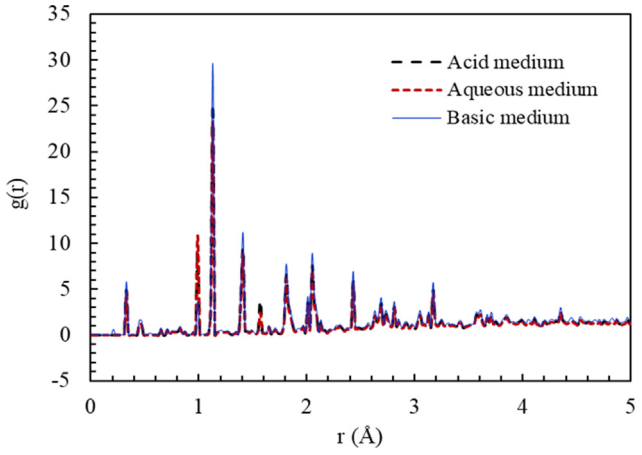


**Fig. 11.** Radial distribution functions of MB11 dye on PANI (001) surface in three solutions.

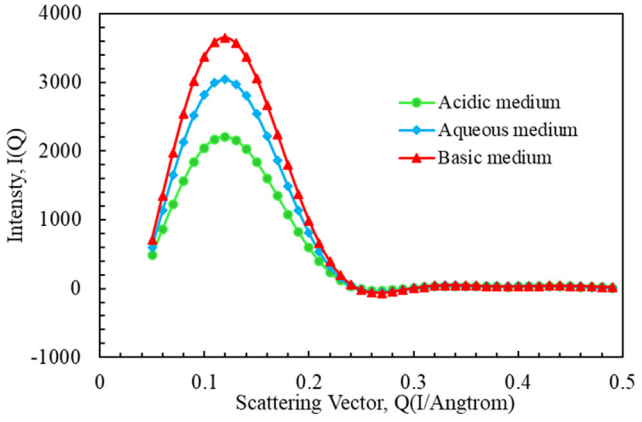


**Fig. 12.** Forcite Analysis-X ray Intensity vs Scattering Vector.

**Table 6**
Adsorption energies of MB11 on the PANI surface in acidic, neutral and basic mediums.

| $E_{Total}$ | $E_{Ads}$ | RAE | $E_{Def}$ | $dE_{Ads}/dNi_{MB\ 11}$ | $dE_{Ads}/dNi_{H2O}$ | $dE_{Ads}/dNi^{+}_{H3O}$ | $dE_{Ads}/dNi^{-}_{OH}$ |
|---|---|---|---|---|---|---|---|
| PANI (001)/MB/125$H_3O^+$, 125$Cl^-$ (acidic medium) | | | | | | | |
| −481.923 | −1202.562 | −638.343 | −564.219 | −100.136 | – | −5.669 | – |
| PANI (001)/MB/250$H_2O$ (neutral medium) | | | | | | | |
| −366.125 | −709.264 | −523.949 | −185.315 | −105.141 | −1.306 | – | – |
| PANI (001)/MB/125$HO^-$, 125$Na^+$ (basic medium) | | | | | | | |
| −92.460 | −291.409 | −249.296 | −42.114 | −92.342 | – | – | −0.318 |

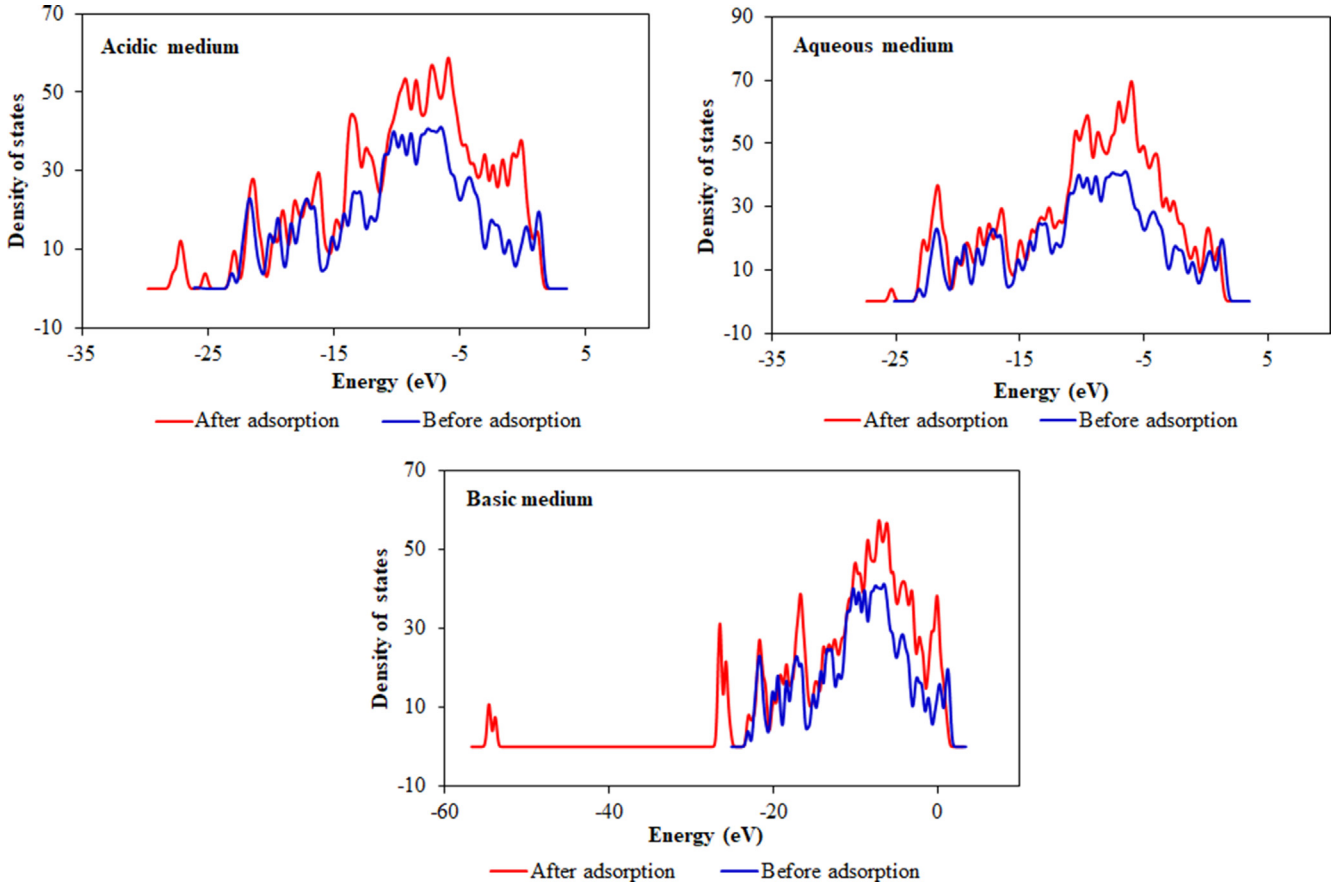


**Fig. 13.** DOS for isolated PANI surface and adsorbed complexes in acidic, neutral and basic mediums.

The values of the different energies of MB11 adsorption onto the PANI are presented in Table 6. The RAE (rigid adsorption energy) represents the energy released when the adsorbed MB11 is not released prior to the geometry optimization step. The deformation energy ($E_{Def}$) reflects the energy released when the adsorbed dye is released on the PANI (001) surface. The high value of deformation energy suggests that the conformational rearrangement caused by MB11 adsorption leads to a stable MB11 molecule and PANI surface.

The highest negative value of the adsorption energy indicates the spontaneity and the high stability of the adsorptive system [81,82]. In addition, the maximum value of adsorption energy (-1202.56 kcal/mol) shows that MB11 adsorption in an acidic medium is adsorbed in the presence of the $H_3O^+$ molecules on the PANI substrate, and electron sharing between the heteroatoms is due to the presence of free doublets on the nitrogen and oxygen atoms, resulting in the overlap of the larger adsorption. The desorption energy (dEads/ dNi) represents the energy of the adsorbate–sub-

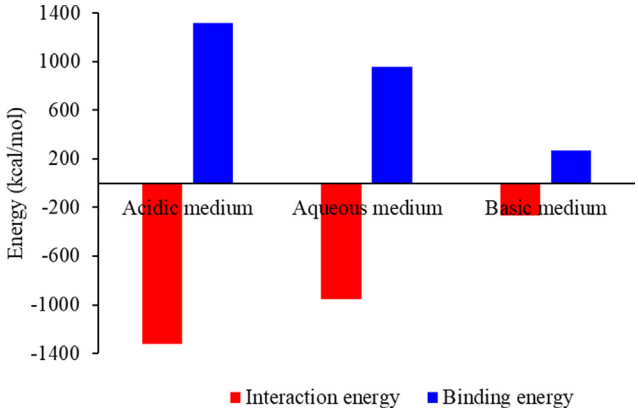


**Fig. 14.** Interaction and binding energies of the complex (MB11-PANI) (in kcal/mol) in acidic, neutral and basic mediums.

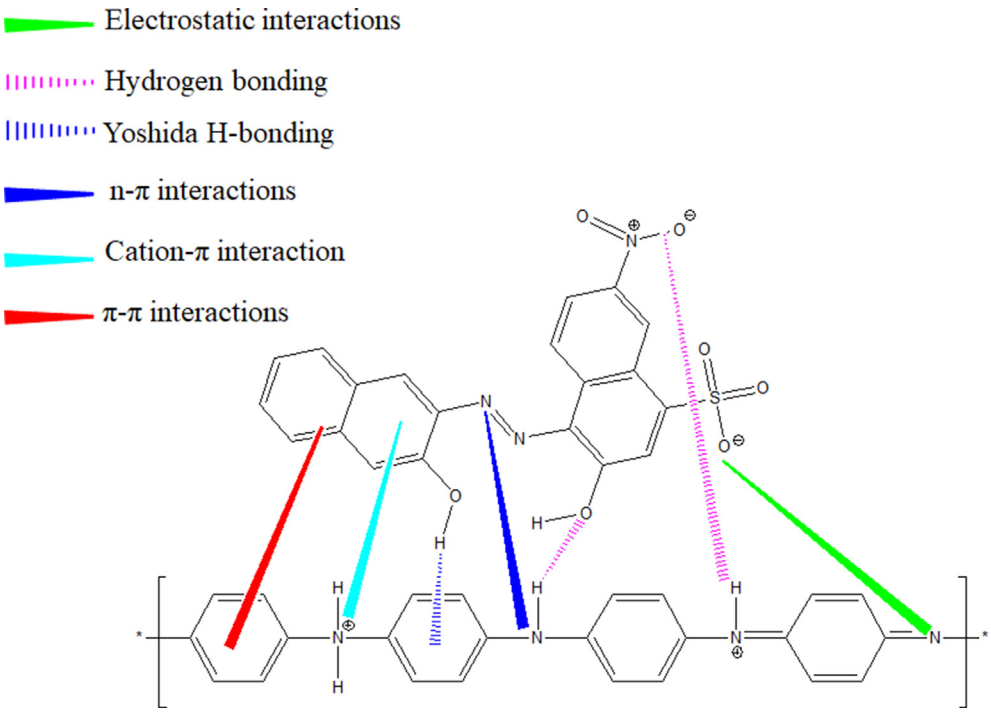


**Fig. 15.** Adsorption mechanisms of MB11 over PANI.

strate configuration where one of the adsorbed molecules has been released. The dynamic modeling analysis confirmed that the PANI is more efficient for removing anionic dye, which confirms the experimental data.

### 3.9. Density of states analysis

To better understand the electronic interactions between MB11 and the PANI (001) surface, the density of state (DOS) of the surface atoms in the most stable adsorption configuration was calculated. The DOS of the unit cell (in electrons/eV) for PANI and the adsorbed complexes in acidic, neutral, and basic media are illustrated in Fig. 13. In the case of adsorption, the DOS peaks of the complexes move to the left, indicating a lowering of energy level. Furthermore, the intensities of the shifted peaks are found to be bigger than those of the isolated PANI surface. A large change in DOS for complex can be observed in the range of −25 to −60 eV, in the basic medium, which indicates that the adsorption of the MB11 on the surface of PANI (001) imposes an important influence on its electronic properties. Also, the polarity of the DOS at any point in the graph defines the bonding behavior of the orbitals at that point. A positive DOS value represents a bonding character for the molecular orbitals (MOs) [83]. A conclusion can be drawn that MB11 molecule adsorption on the polyaniline surface can cause a change in the density of states.

### 3.10. Interaction energies

The nature of the interaction between MB11 and the PANI substrate was highlighted by using the molecular dynamic method as implemented in the Forcite module of the Material Studio software. Fig. 14 shows the interaction and binding energies of the complexes (MB11-PANI) in acidic, neutral and basic media.

The high negative values of interaction energies for the three media suggest that MB11 can strongly adsorb onto the PANI (001) surface. We can see that the MB11 molecule has a higher interaction energy in the acidic medium than in the other mediums. The highest positive value of the binding energy can be assigned to the most stable and best adsorption process [84]. Based on the binding energy values obtained from the molecular dynamic calculation, the adsorption capacity of anionic dye on PANI surface in three media can follow the order: acidic > neutral > basic. This ranking is also compatible with experimental findings. The proposed adsorption mechanisms of the MB11 dye on PANI, based on both theoretical and experimental results are shown in Fig. 15.

## 4. Conclusion

In this research, polyaniline was prepared using in-situ polymerization (PANI/TA) and emulsion polymerization method in the presence of HTAB surfactant (PAN/HTAB). Polyaniline with uniform nanorods structure was obtained when using HTAB as a structure-directing agent. The comparison between the adsorption performances of PANI/HTAB and PANI/TA indicated that PANI/HTAB exhibited a higher removal efficiency for MB11 than PANI/TA. Isotherm data are more fitted to the Freundlich model. Maximum adsorption capacities of 232 mg/g and 115.9 were obtained for PANI/HTAB and PANI/TA, respectively. The thermodynamic study indicated a feasible, endothermic, and spontaneous adsorption process. The pseudo second order model better elucidates the adsorption kinetics. The quantum chemical descriptors calculations are well correlated to the experimental data. Moreover, MD simulations show that MB11 dye is adsorbed on the PANI (001) surface in a nearby parallel position. This encouraging result demonstrated that PANI/HTAB could be used as an effective and recyclable adsorbent to remove MB11 dye from aqueous media.

## CRediT authorship contribution statement

**H. Hajjaoui:** Conceived and designed the experiments, Performed the experiments, Analyzed and interpreted the data, Co-Writing: original draft. **M. Khnifira:** Performed the calculations,

Analyzed and interpreted the data, Co-Writing:original draft. **A. Soufi:** Analyzed and interpreted the data, Co-Writing: original draft. **M. Abdennouri:** Conceived and designed the calculations, Analyzed and interpreted the data; Data curation. **S. Kaya:** Conceived and designed the calculations; Analyzed and interpreted the data. **R. Akkaya:** Analyzed and interpreted the data; Data curation. **N. Barka:** Supervision, Analyzed and interpreted the data; Writing: review and editing, Validation, Funding acquisition.

## Data availability

Data will be made available on request.

## Declaration of Competing Interest

The authors declare that they have no known competing financial interests or personal relationships that could have appeared to influence the work reported in this paper.

## References


[1] A. Soufi, H. Hajjaoui, R. Elmoubarki, M. Abdennouri, A. Qourzal, N. Barka, Appl. Surf. Sci. Adv. 6 (2021), https://doi.org/10.1016/j.apsadv.2021.100145 100145.
[2] J. Mittal, J. Environ. Manage. 295 (2021). https://doi10.1016/j.jenvman.2021.113017 113017.
[3] V.K. Gupta, S. Agarwal, R. Ahmad, A. Mirza, J. Mittal, Int. J. Biol. Macromol. 158 (2020) 1310–1318, https://doi.org/10.1016/j.ijbiomac.2020.05.025.
[4] J. Mittal, A. Mariyam, F. Sakina, R.T. Baker, A.K. Sharma, A. Mittal, J. Clean. Prod. 321 (2021), https://doi.org/10.1016/j.jclepro.2021.129060 129060.
[5] A. Mariyam, J. Mittal, F. Sakina, R.T. Baker, A.K. Sharma, Desalin. Water Treat. 223 (2021) 425–433. https://doi: 10.5004/dwt.2021.27147.
[6] I. Khuranaa, A.K. Shaw, J.M. Bharti, P.K. Khurana, J.E. Rai, Chem. Eng. 6 (2018) 468–477, https://doi.org/10.1016/j.jece.2017.12.029.
[7] J. Kaur, S. Singhal, Superlattices Microstruct. 83 (2015) 9–21, https://doi.org/10.1016/j.spmi.2015.03.022.
[8] M. Tanzifi, M.T. Yaraki, M. Karami, S. Karimi, A.D. Kiadehi, K. Karimipour, S. Wang, J. Colloid Interface Sci. 519 (2018) 154–173, https://doi.org/10.1016/j.jcis.2018.02.059.
[9] L. Wu, X. Liu, G. Lv, R. Zhu, L. Tian, M. Liu, Y. Li, W. Rao, T. Liu, L. Lia, Sci. Rep. 11 (2021) 1064, https://doi.org/10.1038/s41598-021-90235-1.
[10] J. Mittal, R. Ahmad, A. Mittal, Desalin. Water Treat. 227 (2021) 404–411, https://doi.org/10.5004/dwt.2021.27284.
[11] S. Hamidreza, G. A. M. Ali, Potential Applications of Nanomaterials in Wastewater Treatment: Nanoadsorbents Performance. In: Advanced Treatment Techniques for Industrial Wastewater, edited by Athar Hussain and Sirajuddin Ahmed, IGI Global, 2019, pp. 51-61. https://doi.org/10.4018/978-1-5225-5754-8.ch004.
[12] M. Khnifira, W. Boumya, M. Abdennouri, M. Sadiq, M. Achak, G. Serdaroğlu, S. Kaya, S. Şimşek, N. Barka, Int. J. Biol. Macromol. 166 (2121) 707–721. https://doi.org/10.1016/j.ijbiomac.2020.10.228.
[13] M. Bansal, P.K. Patnala, T. Dugmore, CRGSC. 3 (2020), https://doi.org/10.1016/j.crgsc.2020.100036 100036.
[14] Y. Kaur, T. Jasrotia, T. Jasrotia, R. Kumar, G.R. Chaudhary, S. Chaudhary, Chemosphere 278 (2021), https://doi.org/10.1016/j.chemosphere.2021.130366 130366.
[15] J.K. Sahoo, M. Konar, J. Rathc, D. Kumar, H. Sahoo, J. Mol. Liq. 294 (2019), https://doi.org/10.1016/j.molliq.2019.111596 111596.
[16] H. Hajjaoui, A. Soufi, W. Boumya, M. Abdennouri, N. Barka, J. Compos. Sci. 5 (2121) 233. https://doi.org/10.3390/jcs5090233.
[17] M. Tanzifi, M.T. Yaraki, Z. Beiramzadeh, L.H. Saremif, M. Najafifarda, H. Moradig, M. Mansouria, M. Karamih, H. Bazgir, Chemosphere 255 (2020), https://doi.org/10.1016/j.chemosphere.2020.127052 127052.
[18] R.R. Karri, M. Tanzifi, M.T. Yaraki, J.N. Sahu, J. Environ. Manage. 223 (2018) 517–529, https://doi.org/10.1016/j.jenvman.2018.06.027.
[19] L. Ai, J. Jianga, R. Zhang, Synth. Met. 160 (2010) 762–767, https://doi.org/10.1016/j.synthmet.2010.01.017.
[20] M. Tanzifi, S.H. Hosseini, Asieh D Kiadehi, M. Olazar, K. Karimipour, R. Rezaiemehr, I. Ali, J. Mol. Liq. 244 (2017) 189-200. https://doi.org/10.1016/j.molliq.2017.08.122.
[21] M.M. Ayad, A.A. El-nasr, J. Phys. Chem. C. 114 (2010) 14377–14383, https://doi.org/10.1021/jp103780w.
[22] W. Lyu, M. Yu, J. Feng, W. Yan, Polymer 162 (2019) 130–138, https://doi.org/10.1016/j.polymer.2018.12.037.
[23] M. Maruthapandi, V.B. Kumar, J.H.T. Luong, A. Gedanken, Kinetics, ACS Omega 3 (2018) 7196–7203, https://doi.org/10.1021/acsomega.8b00478.
[24] S. Mondal, U. Rana, P. Das, S. Malik, A.C.S. Appl, Polym. Mater. 1 (2019) 1624–1633, https://doi.org/10.1021/acsapm.9b00199.
[25] N. Islam, S. Kaa, CRC Press. (2018), https://doi.org/10.1201/b22471.
[26] I.B. Obot, S. Kaya, C. Kaya, B. Tüzün, Phys. E: Low-Dimens. Syst. Nanostructures 80 (2016) 82–90, https://doi.org/10.1016/j.physe.2016.01.024.
[27] R.G. Parr, L.V. Szentpály, S. Liu, J. Am. Chem. Soc. 121 (1999) 1922–1924, https://doi.org/10.1021/ja983494x.
[28] L.V. Szentpály, S. Kaya, N. Karakuş, J. Phys. Chem. A. 124 (2020) 10897–10908, https://doi.org/10.1021/acs.jpca.0c081962020).
[29] J.L. Gázquez, A. Cedillo, A. Vela, J. Phys. Chem. A. 111 (2007) 1966–1970, https://doi.org/10.1021/jp065459f.
[30] B. Gómez, N.V. Likhanova, M.A. Domínguez-Aguilar, R. Martínez-Palou, A. Vela, J.L. Gazquez, J Phys Chem B 110 (2006) 8928–8934, https://doi.org/10.1021/jp057143y.
[31] Koopmans, T. Über, physica, 1 (1934) 104-113. https://doi.org/10.1016/S0031-8914(34)90011-2.
[32] G. Bahlakeh, M. Ghaffari, M.R. Saeb, B. Ramezanzadeh, F. De Proft, H. Terryn, A J. Phys. Chem. C. 120 (2016) 11014-11026. https://doi.org/10.1021/acs.jpcc.6b03133.
[33] Materials Studio, Revision 8.0, Accelrys Inc., San Diego, USA (2015).
[34] H. Sun, COMPASS, J. Phys. Chem. B 102 (1998) 7338–7364, https://doi.org/10.1021/jp980939v.
[35] H. Bagheri, N. Alipour, Z. Ayazi, Anal. Chim. Acta 740 (2012) 43–49, https://doi.org/10.1016/j.aca.2012.06.026.
[36] D.A. Gopakumar, A.R. Pai, Y.B. Pottathara, D. Pasquini, L.C. de Morais, M. Luke, N. Kalarikkal, Y. Grohens, S. Thomas, A.C.S. Appl, Mater. Interfaces 10 (2018) 20032–20043, https://doi.org/10.1021/acsami.8b04549.
[37] A. Mostafaei, A. Zolriasatein, Prog. Nat. Sci. 22 (2012) 273–280, https://doi.org/10.1016/j.pnsc.2012.07.002.
[38] J. Li, Q. Jia, J. Zhu, M. Zheng, Polym. Int. 55 (2008) 961–969, https://doi.org/10.1002/pi.2353.
[39] X. Zhu, K. Hou, C. Chen, W. Zhang, H. Sun, G. Zhang, Z. Gao, High Perform. Polym. 27 (2015) 227-216. https://doi.org/10.1177%2F0954008314543291.
[40] M. Duhan, R. Kaur, Environ. Technol. 41 (2019) 2977–2990, https://doi.org/10.1080/09593330.2019.1593511.
[41] A. Deb, A. Debnath, N. Bhattacharjee, B. Saha, J. Environ. Anal. Chem. (2020) 1–20, https://doi.org/10.1080/03067319.2020.1843649.
[42] H. Hajjaoui, A. Soufi, M. Abdennouri, S. Qourzal, H. Tounsadi, N. Barka, Appl. Surf. Sci. Adv. 9 (2022), https://doi.org/10.1016/j.apsadv.2022.100263 100263.
[43] M. Farnane, H. Tounsadi, A. Machrouhi, A. Elhalil, F.Z. Mahjoubi, M. Sadiq, M. Abdennouri, S. Qourzal, N. Barka. J. Water Reuse Desalin. 8 (2018) 214-244. https://doi.org/10.2166/wrd.2017.179.
[44] A. Deb, A. Debnath, B. Saha, J. Dispers. Sci. Technol. 42 (2020) 1579–1592, https://doi.org/10.1080/01932691.2020.1775093.
[45] V. Javanbakht, R. Shafiei, Int. J. Biol. Macromol. 152 (2020) 990–1001, https://doi.org/10.1016/j.ijbiomac.2019.10.185.
[46] K. Tul Kubra, M.S. Salman, Md. N. Hasan, J. Mol. Liq. 328 (2021) 115468. https://doi.org/10.1016/j.molliq.2021.115468.
[47] S. Lagergren, Handlingar. 24 (1898) 18981–19039, https://doi.org/10.1007/BF01501332.
[48] Y.S. Ho, G. McKay, Process Biochem. 34 (1999) 451–465, https://doi.org/10.1016/S0032-9592(98)00112-5.
[49] P. Shanmugama, W. Wei, K. Qian, Z. Jiang, J. Lu, J. Xie, Mater. Sci. Eng. B. 248 (2019), https://doi.org/10.1016/j.mseb.2019.114387 114387.
[50] M. Zubair, N. Jarrah, M.S. Manzar, M. Al-Harthi, M. Daud. N.D. Mu'azu, S. A. Haladuf, J. Mol. Liq. 230 (2017) 344–352. https://doi.org/10.1016/j.molliq.2017.01.031.
[51] W.J. Weber, J.C. Morris, J. Sanit. Eng. Div. 89 (1963) 31–59, https://doi.org/10.1061/JSEDAI.0000430.
[52] X. Zhang, Y. Li, M. Li, H. Zheng, Q. Du, H. Li, Y. Wang, D. Wang, C. Wang, K. Sui, H. Li, Y. Xia, J. Colloid Interface Sci. 556 (2019) 249–257, https://doi.org/10.1016/j.jcis.2019.08.037.
[53] I. Langmuir, J. Am. Chem. Soc. 38 (1916) 2221–2295, https://doi.org/10.1021/ja02268a002.
[54] T.W. Webi, R.K. Chakravort, AlChE Journal 20 (1974) 228–238, https://doi.org/10.1002/aic.690200204.
[55] H. Freundlich, J. Phy, Chem 57 (1906) 385–470.
[56] M.A. Moosavian, N. Moazezi, Desalin. Water Treat. 57 (2016) 20817–20836, https://doi.org/10.1080/19443994.2015.1110717.
[57] M. Manes, L.J.E. Hofer, J. Phys. Chem. 73 (1969) 584–590, https://doi.org/10.1021/j100723a018.
[58] A. Naga Babu, D.S Reddy, G.S Kumar, K. Ravindhranath, G.V.K. Mohan, J. Environ. Manage. 218 (2018) 602-612. https://doi.org/10.1016/j.jenvman.2018.04.091.
[59] F. Banisheykholeslami, M. Hosseini, G.N. Darzi, Int. J. Biol. Macromol. 177 (2021) 306–316, https://doi.org/10.1016/j.ijbiomac.2021.02.118.
[60] A. Muhammad, A.H.A. Shah, S. Bilal, Appl. Sci. 10 (2020) (2020) 2882, https://doi.org/10.3390/app10082882.
[61] M. Min, L. Shen, G. Hong, M. Zhu, Y. Zhang, X. Wang, Y. Chen, B.S. Hsiao, Chem. Eng. J. 197 (2012) 88–100, https://doi.org/10.1016/j.cej.2012.05.021.
[62] W. Boumya, M. Khnifira, A. Machrouhi, M. Abdennouri, M. Sadiq, M. Achaq, G. Serdaroğlu, S. Kaya, S. Şimşek, N. Barka, J. Mol. Liq. 331 (2021), https://doi.org/10.1016/j.molliq.2021.115706 115706.
[63] S. Charafi, F.Z. Janani, A. Elhalil, M. Abdennouri, M. Sadiq, N. Barka, Biointerface Res, Appl. Chem. 13 (3) (2023) 265. https://doi.org/10.33263/BRIAC133.265.
[64] M. Daniel G. de Luna, E.D. Flores, D.A.D. Genuino, C.M. Futalan, M.W. Wan, J. Taiwan Inst. Chem. Eng. 44 (2013) 646-653. https://doi.org/10.1016/j.jtice.2013.01.010.

[65] G. Sriram, U.T. Uthappa, R.M. Rego, M. Kigga, T. Kumeria, H.Y. Jung, M.D. Kurkuri, Chemosphere 238 (2020), https://doi.org/10.1016/j.chemosphere.2019.124692 124692.
[66] S. Kaushal, R. Badru, S. Kumar, H. Kaur, P. Singh, J. Inorg. Organomet. Polym. Mater. 28 (2018) 968–977, https://doi.org/10.1007/s10904-018-0817-8.
[67] S. Mishra, S.S. Sahoo, A.K. Debnath, K.P. Muthe, N. Das, P. Parhi, Adv. Powder Technol. 31 (2021) 4552–4562, https://doi.org/10.1016/j.apt.2020.10.001.
[68] M. Essandoh, R.A. Garcia, Chemosphere 206 (2018) 502–512, https://doi.org/10.1016/j.chemosphere.2018.04.182.
[69] I. Khuranaa, A.K. Shaw, J.M. Bharti, P.K. Khurana, J.E. Raia, Chem. Eng. 6 (2018) 468–477, https://doi.org/10.1016/j.jece.2017.12.029.
[70] A. Khalid, M. Zubair, Ihsanullah, Arab. J. Sci. Eng. 43 (2018) 2167–2179, https://doi.org/10.1007/s13369-017-2543-x.
[71] F.J. Luque, J.M. López, M. Orozco, Theor. Chem. Acc. 103 (2001) 343–345, https://doi.org/10.1007/s002149900013.
[72] S. Lakshminarayanan, V. Jeyasingh, K. Murugesan, N. Selvapalam, G. Dass, J. Photochem. Photobiol. 6 (2021), https://doi.org/10.1016/j.jpap.2021.100022 100022.
[73] N. Chafai, S. Chafaa, K. Benbouguerra, D. Daoud, A. Hellal, M. Mehri, J. Taiwan Inst. Chem. Eng. 70 (2017) 331–344, https://doi.org/10.1016/j.jtice.2016.10.026.
[74] I.B. Obot, N.O. Obi-Egbedi, S.A. Umoren, Int. J. Electrochem. Sci. 4 (2009) 863–877.
[75] S. Kaya, C. Kaya, Comput, Theor. Chem. 1060 (2015) 66–70, https://doi.org/10.1016/j.comptc.2015.03.004.
[76] R.G. Pearson, Acc. Chem. Res. 26 (1993) 250–255, https://doi.org/10.1021/ar00029a004.
[77] P.K. Chattaraj, H. Lee, R.G. Parr, J. Am. Chem. Sot. 113 (1991) 1855–1856, https://doi.org/10.1021/ja00005a073.
[78] P.K. Chattaraj, S. Sengupta, J. Phys. Chem. 100 (1996) 16126–16130, https://doi.org/10.1021/jp961096f.
[79] E. Chamorro, P.K. Chattaraj, P. Fuentealba, J. Phys. Chem. A. 107 (2003) 7068–7072, https://doi.org/10.1021/jp035435y.
[80] J.P. Zeng, J.Y. Zhang, X.D. Gong, Comput, Theor. Chem. 963 (2011) 110–114, https://doi.org/10.1016/j.comptc.2010.10.006.
[81] M. Khnifira, S. El Hamidi, A. Machrouhi, A. Mahsoune, W. Boumya, H. Tounsadia, F.Z. Mahjoubi, M. Sadiq, N. Barka, M. Abdennouri, Desalin. Water Treat. 190 (2020) 393–411, https://doi.org/10.5004/dwt.2020.25737.
[82] M. Khnifira, A. Mahsoune, M.E. Belghiti, L. Khamar, M. Sadiq, M. Abdennouri, N. Barka, Mater. Today Proc. 37 (2020) 3987–3993, https://doi.org/10.1016/j.matpr.2020.10.797.
[83] D.J. Arenas, C. Middleton, A.F. Kemper, Phys. Rev. B. 91 (2015), https://doi.org/10.1103/PhysRevB.91.144103 144103.
[84] M. Khnifira, A. Mahsoune, M.E. Belghiti, L. Khamar, M. Sadiq, M. Abdennouri, N. Barka, CRG SC. 4 (2021), https://doi.org/10.1016/j.crgsc.2021.100085 100085.